Available online at www.sciencedirect.com
ScienceDirect
International Journal of Thermal Sciences 48 (2009) 440–448
International Journal of Thermal Sciences
www.elsevier.com/locate/ijts

Temperature and pressure dependent effective thermal conductivity of fibrous insulation

Shu-yuan Zhao *, Bo-ming Zhang, Xiao-dong He

Center for Composite Materials and Structure, Harbin Institute of Technology, Harbin 150080, China

Received 18 September 2007; received in revised form 12 May 2008; accepted 13 May 2008

Available online 13 June 2008

Abstract

In present paper, a numerical model combined radiation and conduction heat transfer was developed to predict the effective thermal conductivity of fibrous insulation at various temperatures and pressures. Effective thermal conductivities of the fibrous insulation were measured over a wide range of temperature (300–973 K) and pressure (10^{-2}–10^5 Pa) using a developed apparatus. The transmittance spectra in the wavelength range of 2.5–25 μm were also measured at temperatures up to 973 K using a Fourier Transform Infrared Spectrometer. From transmittance data, the spectral extinction coefficients and Rosseland mean extinction coefficients were obtained at various temperatures to investigate the radiative heat transfer in fibrous insulation. The numerical and experimental data were compared. It was found that the calculated values corresponded with the experimental values within an average of 14.7 percent. Numerical results were consistent with experimental results throughout the investigated environmental conditions.

Keywords: Effective thermal conductivity; Transmission; Extinction coefficient; Insulation

1. Introduction

Space transportation vehicles will encounter aerodynamic heating when entering the earth's atmosphere at hypersonic speeds. Metallic thermal protection system (TPS), which consists of a metallic shell panel fabricated from high temperature alloy and lightweight insulation, is used to limit the maximum temperature of the primary structure of the vehicle during reentry. Many design options have the potential to improve the thermal performance of metallic TPS. An obvious way is to develop more efficient non-load-bearing insulation. High temperature fibrous insulation is a good candidate being considered for use in the metallic TPS since it provides an excellent combination of low weight, low thermal conductivity and high service temperature. However, limited information is available on the thermal properties of insulation under the environmental conditions to which re-entry type vehicles are exposed. Earth re-entry typically produces aerodynamic heating to a surface to the temperature as high as 1273 K in a pressure range from 1.333 to 1.013×10^5 Pa [1]. Heat transfer through a fibrous insulation involves combined modes of heat transfer: solid conduction, gas conduction, natural convection and radiation. The relative contributions of the different heat transfer modes vary during re-entry. The complex heat transfer makes the analysis and the design of insulation quite difficult.

Over the past several decades, significant advances have been made in the understanding of fundamental properties of fibrous insulation [2–5], experimentally and analytically. Lee and Cunnington [2] have provided a comprehensive review of heat transfer in general porous material. The researchers [3,4] have developed an effective thermal conductivity model based on superposition of gas, solid and apparent radiation thermal conductivities, based on optically thick assumption, and compared the results with measured effective thermal conductivities of samples subjected to certain temperature difference across the insulation thickness over a wide range of environmental pressures. Tong et al. [6,7] used the two-flux model assuming a linearized anisotropic scattering to model radiation heat transfer through fibrous insulation, and the predicted fluxes which combined radiant and conduction were compared with measured data up to

* Corresponding author.
E-mail address: angel.zsy@126.com (S.-y. Zhao).

1290-0729/$ – see front matter
doi:10.1016/j.ijthermalsci.2008.05.003

Nomenclature

c	speed of light in the medium	$\mathrm{m\,s^{-1}}$
c_p	specific heat of the sample	$\mathrm{J\,kg^{-1}\,K^{-1}}$
D_f	diameter of fibers	m
d_g	gas collision diameter	m
E_b	blackbody emissive power	$\mathrm{W\,m^{-2}}$
$E_{b\lambda}$	spectral blackbody emissive power	$\mathrm{W\,m^{-2}}$
f	solid fraction ratio	
h	Plank's constant	J s
K	Boltzmann constant	$\mathrm{J\,K^{-1}}$
k_c	thermal conductivity due to conduction	$\mathrm{W\,m^{-1}\,K^{-1}}$
k_e	effective thermal conductivity	$\mathrm{W\,m^{-1}\,K^{-1}}$
k_g	gas thermal conductivity	$\mathrm{W\,m^{-1}\,K^{-1}}$
k_g^*	gas thermal conductivity at an atmospheric pressure	$\mathrm{W\,m^{-1}\,K^{-1}}$
$\bar{k}_r$	mean radiative thermal conductivity	$\mathrm{W\,m^{-1}\,K^{-1}}$
K_R	Rosseland mean extinction coefficient	$\mathrm{m^{-1}}$
k_s	solid thermal conductivity	$\mathrm{W\,m^{-1}\,K^{-1}}$
k_s^*	fiber parent material	$\mathrm{W\,m^{-1}\,K^{-1}}$
L	insulation thickness	m
L_c	characteristic length for gas conduction	m
m	exponent for solid conduction	
n	the index of refraction	
p	pressure	Pa
Pr	Prandtl number	
q	heat flux	$\mathrm{W\,m^{-2}}$
q_r''	the radiant heat flux	$\mathrm{W\,m^{-2}}$
t	time	s
T	temperature	K
T_1	hot side temperature	K
T_2	cold side temperature	K
$T_{n\lambda}$	spectral transmittance	
x	spatial coordinate through the insulation thickness	m

Greek symbols

α	thermal accommodation coefficient	
β_λ	spectral extinction coefficient	$\mathrm{m^{-1}}$
$\bar{\gamma}$	gas specific heat ratio	
λ	wavelength	m
λ_m	molecular mean free path	m
ρ	density	$\mathrm{kg\,m^{-3}}$
σ	Stefan–Boltzmann constant	$\mathrm{W\,m^{-2}\,K^{-4}}$

Subscripts

b	blackbody
g	gas
s	solid

450 K at one atmosphere. Daryabeigi [8] modeled heat transfer in alumina fibrous insulation to predict the effective thermal conductivities. The predicted results were compared with the experimental data at gas pressures between 10^{-2} Pa and 10^5 Pa and temperatures up to 1273 K.

In this work, the effective thermal conductivity of the fibrous insulation is measured over a wide range of temperature (300–973 K) and pressure (10^{-2}–10^5 Pa) using a developed apparatus. To characterize the contribution of radiative heat transfer in the fibrous insulation, the spectral transmittances in the wavelength range of 2.5–25 μm are measured over the temperature range of 291–973 K using a Fourier Transform Infrared Spectrometer, which are then used to determine the spectral extinction coefficient as well as Rosseland mean extinction coefficient. The effective thermal conductivity of the fibrous insulation is calculated from a numerical heat transfer model. The numerical results were compared with the steady-state experimental results.

2. Theoretical analysis

Heat transfer through a fibrous insulation involves combined modes of heat transfer: solid conduction through fibers, gas conduction and natural convection in the space between fibers, and radiation interchange through participating media. Natural convection heat transfer in porous media is negligible [9]. Therefore, the conservation of energy for one dimensional heat transfer in the insulation by conduction and radiation yields the partial differential equation [10].

$$\rho c_p \frac{\partial T}{\partial t} = \frac{\partial}{\partial x}\left(k_c \frac{\partial T}{\partial x}\right) - \frac{\partial q_r''}{\partial x} \tag{1}$$

Subjected to the following initial and boundary conditions:

$$T(x,0) = T_0 \tag{2}$$

$$T(0,t) = T_1 \tag{3}$$

$$T(L,t) = T_2 \tag{4}$$

In the present study, the optical thickness (optical thickness is the product of the extinction coefficient and thickness of the sample) of the insulation is larger than 180 from the experimental results, which is large enough for the sample to be treated as an optically thick medium. Therefore, the radiation in the insulation can be considered as a diffusion process, and the radiation heat flux, q_r'', can be reduced to [11]:

$$q_r'' = -\frac{16n^2\sigma}{3K_R}T^3\frac{\partial T}{\partial x} \tag{5}$$

It can be stated that the index of refraction is assumed to be unity for the current analysis. Then the local effective thermal conductivity, k_e, is defined as

$$k_e = k_c + \frac{16\sigma}{3K_R}T^3 \tag{6}$$

The first term in Eq. (6) represents the thermal conductivity due to solid and gas conduction, and the last term represents

"radiative conductivity" based on the Rosseland diffusion approximation.

Several theories have been developed to describe the combined conduction thermal conductivity due to solid conduction and gas conduction. In the present study, two thermal resistances in a parallel arrangement are used for modeling heat transfer in fibrous insulation [12]

$$k_c = f k_s + (1 - f) k_g \tag{7}$$

The effect of pressure on the thermal conductivity of a gas can be investigated by the way of the Maxwell moment method [13,14] and temperature jump theory [15]. Daryabeigi used temperature jump theory to model the gas conduction in fibrous insulation, and the gas thermal conductivity is described as [12]

$$k_g = \frac{k_g^*}{1 + 2(2-\alpha)/\alpha(2\bar{\gamma}/(\bar{\gamma}+1))(1/Pr)\lambda_m/L_c} \tag{8}$$

the molecular mean free path, λ_m, which is given by [16]

$$\lambda_m = \frac{KT}{\sqrt{2}\pi d_g^2 P} \tag{9}$$

and L_c is given by

$$L_c = \frac{\pi}{4}\frac{D_f}{f} \tag{10}$$

The empirical model for solid conduction can be defined as

$$k_s = f^m k_s^* \tag{11}$$

the above equation is based on the model proposed by Verschoor et al. [3]. Hager and Steere [4] used $m = 3$ to model the solid conduction in fibrous insulation and stated that it was an upper limiting value when contact with the fibers was less than perfect. $m = 2$ was utilized for modeling solid conduction in fibrous insulation spacers in high temperature multilayer insulations [12]. For alumina fibrous insulation, $m = 1.4$ was determined using a parameter estimation technique in Ref. [17]. In the present investigation, $m = 2$ is used.

The measured Rosseland mean extinction coefficient was substituted in the Eq. (6) to solve the radiation heat transfer in fibrous insulation. The values of α, $\bar{\gamma}$, Pr and d_g used in the calculation of gas conduction are provided in Ref. [1]. $D_f = 5$ μm is used for the current analysis. The density of the fiber parent material is 2600 kg/m^3. $k_s^* = 0.24623 + 0.00149T$ W/(m K) was used to calculate the solid thermal conductivity [18]. The measured steady-state temperatures on the top and bottom of the sample were used as boundary conditions. A linearly varying temperature distribution through the thickness of the sample was selected as the initial condition. Eq. (1) was solved numerically using a finite difference technique until the temperature at each volume element did not change with successive iterations and the steady state conditions were achieved. The heat flux at steady-state conditions was used to calculate the effective thermal conductivity.

3. Experiments

3.1. Sample description

In the present study, the sample is high-alumina fibrous insulation. Its primary components are alumina and silica. The nominal density is 128 kg/m^3. The SEM micrograph of fibrous insulation sample is shown in Fig. 1. From the figure it can be seen that the fiber diameter varies from 1 μm to 9 μm, approximately.

3.2. Effective thermal conductivity

Effective thermal conductivity which combines the effects of heat transfer by conduction, convection and radiation, is one of the most important parameters to characterize the thermal performance of the insulation. Effective thermal conductivity varies with temperature and pressure under the aerodynamic heating conditions. In order to investigate the heat transfer through the fibrous insulation and obtain the effective thermal conductivity exactly and reliably, an apparatus was developed. A schematic of the apparatus is shown in Fig. 2. A graphite radiant heater is used as the radiant heat source and a temperature as high as 1873 K can be reached. The sample is placed between a septum plate and a water-cooled plate maintained at room temperature. The water-cooled plate is placed on the bottom to reduce the effect of natural convection. The insulating screen and guarded insulation are used to minimize lateral heat loss and produce a more uniform heating of the overall test setup. Eight type K thermocouples are installed to monitor the change of temperatures during heating, four thermocouples for the hot side and the others for the cold side. Two heat flux gauges (WYP hard probe type) located on the water-cooled plate are used to measure the flux of heat energy flowing through the sample. Layouts of thermocouples and heat flux gauges on water-cooled plate and septum plate are shown in Figs. 3 and 4. Only the thermocouple and heat flux gauge data from the central 300 × 300 mm section of the test setup are used to calculate the effective thermal conductivity of the sample. All the measured data are collected using

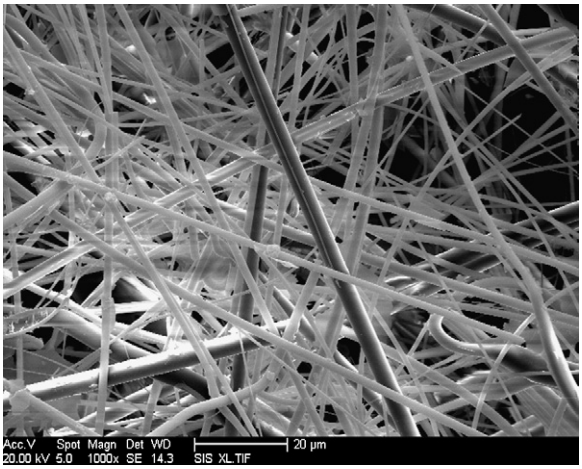

Fig. 1. SEM micrograph of fibrous insulation sample.

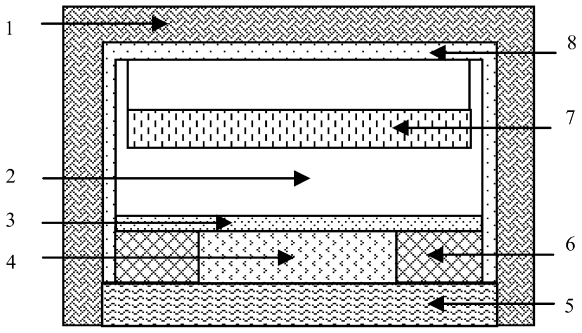

Fig. 2. Schematic of the thermal conductivity apparatus. 1. Carbon fabric insulation barrel; 2. Vacuum chamber; 3. Septum plate; 4. Test specimen; 5. Water-cooled plate; 6. Guarded insulation; 7. Graphite radiant heater; 8. Insulating screen.

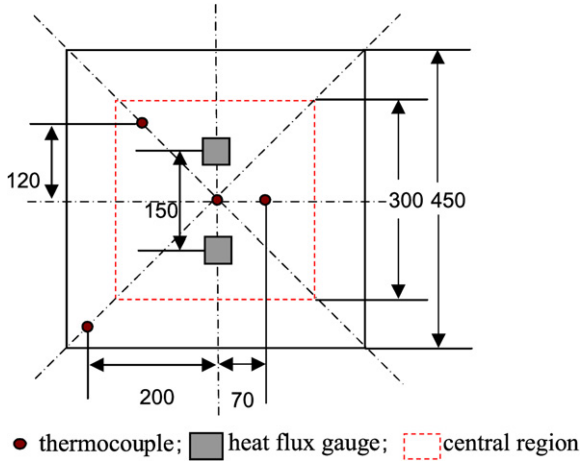

Fig. 3. Layout of thermocouples and heat flux gauges on water-cooled plate.

a multi-channel temperature measurement device in conjunction with a personal computer-based data acquisition software. The apparatus is housed inside a vacuum chamber and the environmental pressure varies from 10^{-2} to 10^{5} Pa. A pressure sensor is used to measure the pressure in the vacuum chamber. Once the insulation sample is inserted into the test apparatus, the gas inside the vacuum chamber is removed. The primary reason for which nitrogen is selected for use in this experiment is to eliminate water vapor in air from the chamber and reduce the oxidation of the graphite at higher temperature. Once all the thermocouples on the hot side and cold side and heat flux gages on the water-cooled plate are stabilized, data storage is initiated. Using the measured heat flux, the hot side temperature, the cold side temperature, and the sample thickness, the effective thermal conductivity of the insulation sample can be calculated from Fourier's law of heat conduction:

$$k_e = \frac{qL}{T_1 - T_2} \tag{12}$$

The uncertainty of the measured effective thermal conductivity is estimated from the error propagation equation of Eq. (13).

$$\frac{\delta k}{k_e} = \left(\left(\frac{\delta q}{q}\right)^2 + \left(\frac{\delta L}{L}\right)^2 + \left(\frac{\delta \Delta T}{\Delta T}\right)^2\right)^{0.5} \tag{13}$$

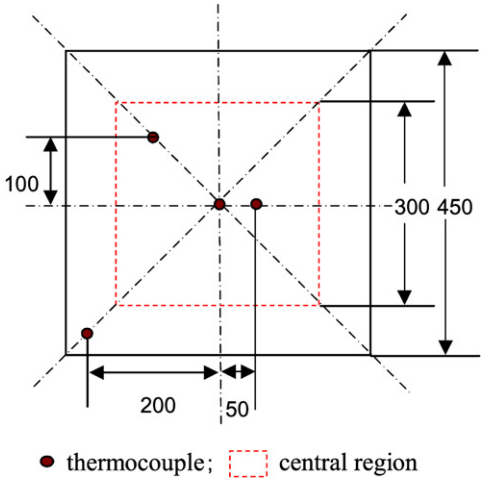

Fig. 4. Layout of thermocouples on septum plate.

The uncertainty for each measurement point is shown in Table 1. The overall uncertainty of the measurement is within 8% approximately.

In the present study, the sample has a square cross sectional area with the sides being 450 mm. The nominal thickness of the sample is 40 mm.The effective thermal conductivity of the sample is measured with the nominal hot side temperatures set at 373, 473, 573, 673, 773, 873, 973 K, and the nominal experimental pressures controlled at 1×10^{-2}, 10, 1×10^{2}, 5×10^{3}, 5×10^{4}, 1.013×10^{5} Pa. Each measurement consists of setting temperature the septum plate on the top of the sample to the desired temperature, varying the nitrogen gas to the desired pressure, and allowing both temperature and pressure to reach a steady state condition.

3.3. Rosseland mean extinction coefficient

In order to quantify thermal radiation within the insulation, the temperature-dependent extinction coefficient is needed. Physically, the extinction coefficient represents the decay rate of the radiation intensity passing through the material. Rosseland mean extinction coefficient is a more commonly used material parameter than the spectral extinction coefficient, as the former represents the overall effect of energy decay in the material. The Rosseland mean extinction coefficient is defined as [14]

$$\frac{1}{K_R} = \int_0^\infty \frac{1}{\beta_\lambda} \frac{\partial E_{b\lambda}}{\partial E_b} d\lambda \tag{14}$$

The spectral extinction coefficients for thin sample can be obtained, using Beer's law as [11]:

$$T_{n\lambda} = \exp\left(-\int_0^L \beta_\lambda \, dx\right) \tag{15}$$

For a homogeneous sample, β_λ is independent of the sample thickness, then Eq. (15) can be reduced to

$$\beta_\lambda = -\frac{\ln(T_{n\lambda})}{L} \tag{16}$$

Table 1
The uncertainty of the effective thermal conductivity measurement

Hot side temperature (K)	Pressure					
	1×10^{-2} Pa	10 Pa	1×10^{2} Pa	5×10^{3} Pa	5×10^{4} Pa	1.013×10^{5} Pa
373	7.53	7.44	7.45	7.45	7.44	7.44
473	7.68	7.46	7.48	7.45	7.47	7.49
573	7.51	7.50	7.51	7.52	7.52	7.54
673	7.57	7.52	7.56	7.55	7.55	7.59
773	7.61	7.54	7.59	7.58	7.59	7.62
873	7.61	7.65	7.63	7.58	7.64	7.64
973	7.66	7.58	7.59	7.61	7.64	7.65

For black bodies, the monochromatic emissive power was derived by Planck by introducing the quantum concept for electromagnetic energy as

$$E_{b,\lambda} = \frac{2\pi hc^2}{\lambda^5(\exp(hc/(KT\lambda)) - 1)} \tag{17}$$

Then Eq. (14) can be transformed to:

$$\frac{1}{K_R} = \int_0^\infty -\frac{L}{\ln(T_{n\lambda})} \frac{2\pi h^2 c^3 \exp(hc/(KT\lambda))}{4K\sigma\lambda^6 T^5[\exp(hc/(KT\lambda)) - 1]^2} d\lambda \tag{18}$$

By integrating Planck's law (Eq. (17)) over the wavelength, it has been established that over 80% of the thermal radiation lies in the wavelength range between 2.5 μm and 25 μm below 973 K. In this study, the spectral transmittance is measured for the wavelength range of 2.5–25 μm using a Fourier transform infrared spectrometer (Bruker IFS 66V/S, Germany).

4. Results and discussion

4.1. Effective thermal conductivity

The effective thermal conductivity of the sample as a function of the average temperature is presented in Fig. 5. The effective thermal conductivity increases non-linearly with the increase of the average temperature. The variation of effective thermal conductivity with environmental pressure for the sample is shown in Fig. 6. Data are plotted for three different nominal hot side temperatures. The figure shows that the measured effective thermal conductivity increases with increasing pressure levels. As can be seen, the effective thermal conductivity increases somewhat below 10 Pa, rapidly between 1×10^2 Pa and 5×10^3 Pa and then stays relatively constant above 5×10^4 Pa. As solid and radiative contributions are independent of gas pressure, changing pressure only affects the contribution of gas conduction to the effective thermal conductivity. It can be stated that gas conduction increases with increasing pressure. The same trends are observed for all other insulation sample.

4.2. Rosseland mean extinction coefficient

The measured spectral transmittance as a function of wavelength is plotted in Fig. 7 for high-alumina fibrous insulation

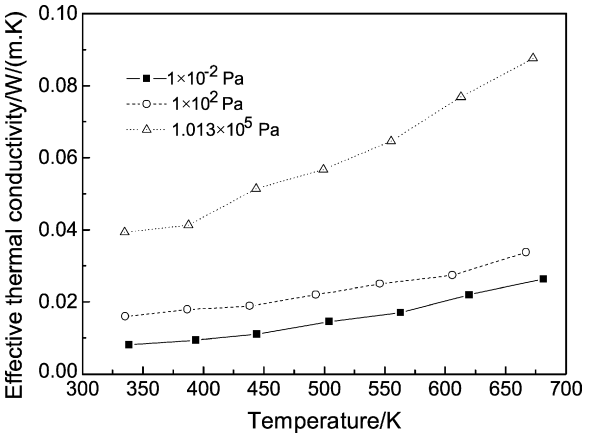

Fig. 5. Variation of effective thermal conductivity with temperature.

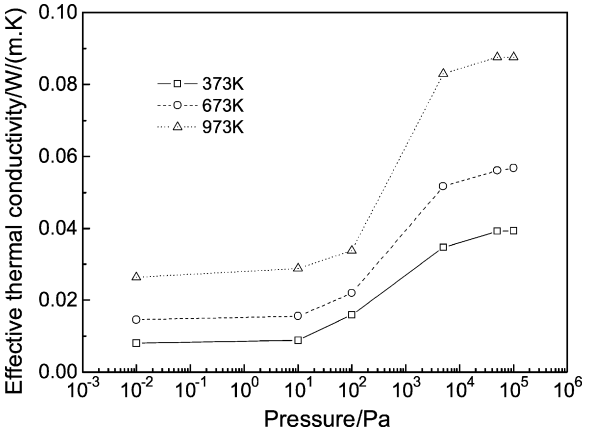

Fig. 6. Variation of effective thermal conductivity with pressure.

with different thicknesses. It demonstrates that the spectral transmittance decreases as the media thickness increases. The insulation transmittance property is strongly dependent upon the spectral wavelength. It is noticed that all the testing samples with different thicknesses exhibit similar dependence upon the wavelength. Fig. 8 shows the variation of spectral transmittance with wavelength at various temperatures. Given the fact that there is no obvious change in the physical and chemical properties of high-alumina fibrous insulation up to 973 K, the trends are similar for the sample at various temperatures. The maximum values of transmittance decrease and show a shift towards the direction of longer wavelength as temperature increases.

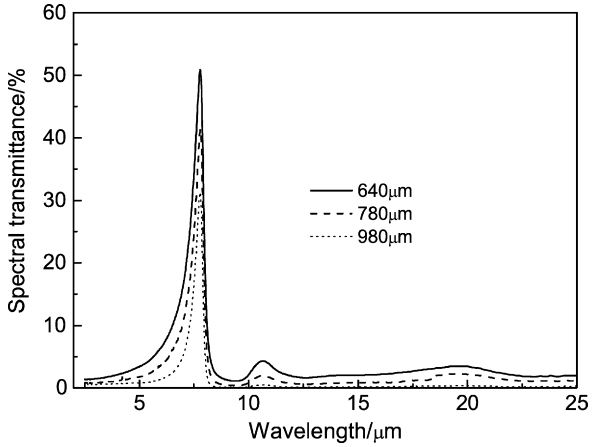

Fig. 7. Variation of spectral transmission of samples with different thicknesses with wavelength at room temperature.

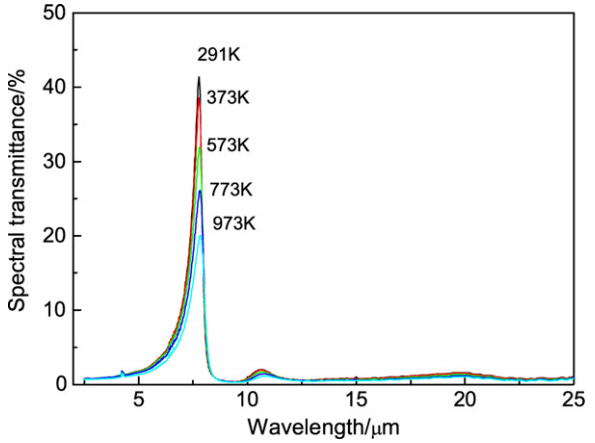

Fig. 8. Variation of spectral transmittance of samples with wavelength at various temperatures.

Spectral extinction coefficient can be obtained from Eq. (16) using the measured spectral transmittance. The spectral extinction coefficient thus determined is plotted as a function of wavelength in Figs. 9 and 10. Fig. 9 shows that the spectral extinction coefficients of the samples with different thicknesses show comparatively large differences in the wavelength range of 2.5 μm to 5.2 μm. The spectral extinction coefficients coincide very well in the range of 5.2 μm to 8 μm. Little differences are shown in the spectral extinction coefficients of the three samples in the range of 8 μm to 25 μm. On the whole, the assumption of spectral extinction coefficient independent of sample thickness is applicable for the samples in the present investigation range. Fig. 10 demonstrates that the spectral extinction coefficients at various temperatures exhibit similar trend. Spectral extinction coefficients increase slightly as temperature increases.

Rosseland mean extinction coefficient is an average extinction coefficient over the spectrum weighted by the emissive power. It represents the ability to eliminate thermal radiation at a certain temperature. The variation of Rosseland mean extinction coefficient with temperature obtained from Eq. (18) is shown in Fig. 11. The results demonstrate that the Rosseland

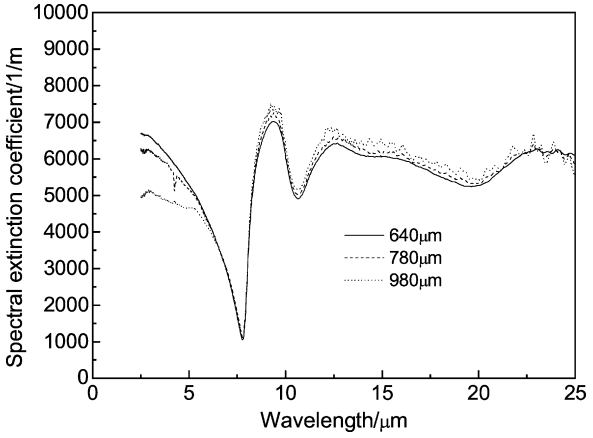

Fig. 9. Variation of spectral extinction coefficient of samples with different thickness with wavelength at room temperature.

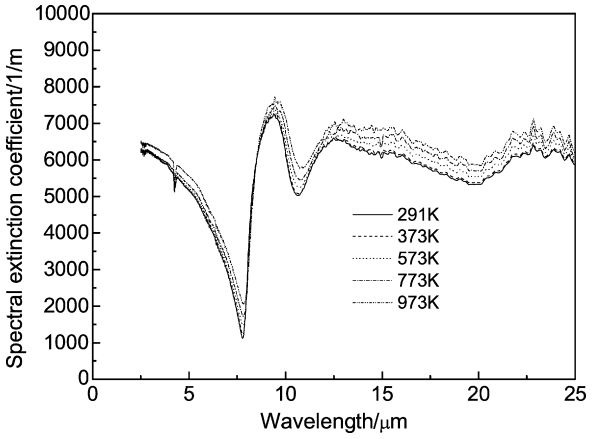

Fig. 10. Variation of spectral extinction coefficient of samples with wavelength at various temperatures.

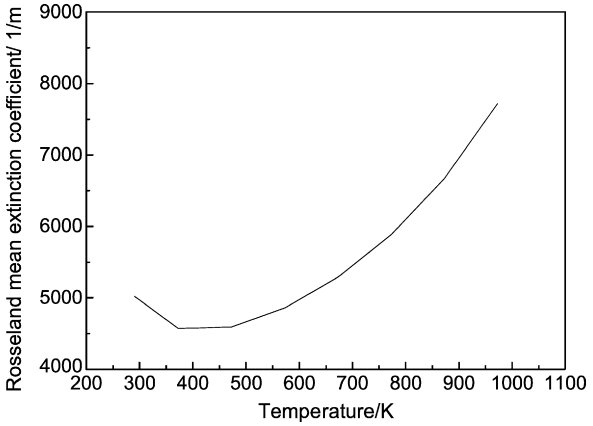

Fig. 11. Variation of Rosseland mean extinction coefficient with temperature.

mean extinction coefficient initially decreases with increasing temperature, reaching the minimum value of 4570 1/m at around 373 K, and then increases with the rise of temperature. It is noticed that if the thickness of the sample is sufficiently large, the optical thickness of the insulation will be large enough for the sample to be treated as an optically thick medium and radiation in the insulation can be considered as a diffusion process.

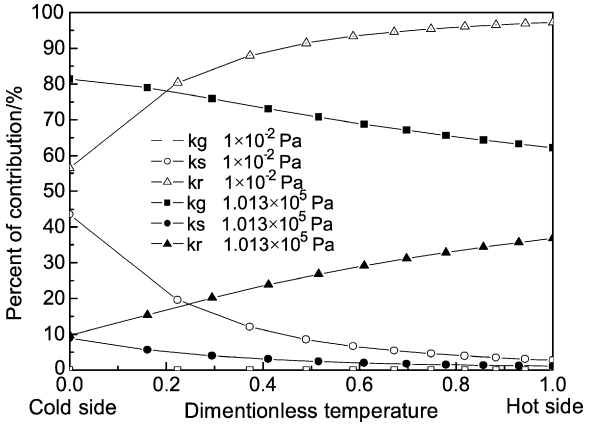

Fig. 12. Percent of contribution of different heat transfer mechanisms to local thermal conductivity at the nominal hot side temperature of 973 K under pressures of 1×10^{-2} Pa and 1.013×10^5 Pa.

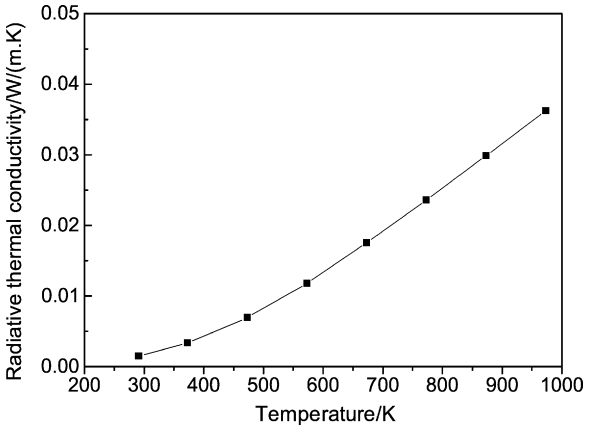

Fig. 13. Variation of radiative thermal conductivity with temperature.

4.3. Numerical results

The various heat transfer mechanisms through fibrous insulation are coupled, and the net contributions of each component to the effective thermal conductivity cannot be independently assessed. The contribution percent of different heat transfer mechanisms to local thermal conductivity at the nominal hot side temperature of 973 K under pressures of 1×10^{-2} Pa and 1.013×10^5 Pa is shown in Fig. 12. The solid conduction, gas conduction and radiation contributions to the local thermal conductivity are presented as a function of the dimensionless temperature. The dimensionless temperatures of 0 and 1 correspond to temperatures of cold side and hot side. The percent of contribution of solid conduction decreases as the temperature increases. Gas conduction is negligible at pressure of 1×10^{-2} Pa. While it has a larger contribution to the thermal conductivity compared to radiation at pressure of 1.013×10^5 Pa. The radiation becomes more dominant with increasing temperature. The contribution of radiation can be up to 90 percent at high temperature at pressure of 1×10^{-2} Pa. The variation of radiative thermal conductivity with temperature for the fibrous insulation sample is presented in Fig. 13. The radiative thermal conductivity increases with the rise of temperature non-linearly.

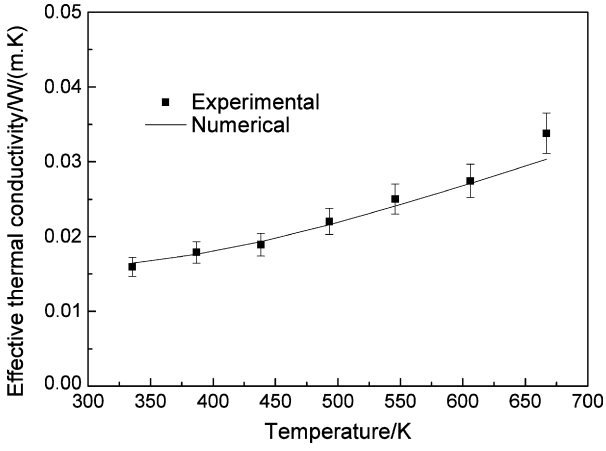

(a)

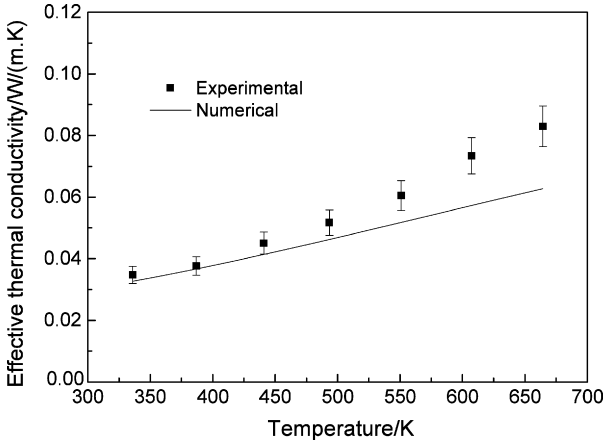

(b)

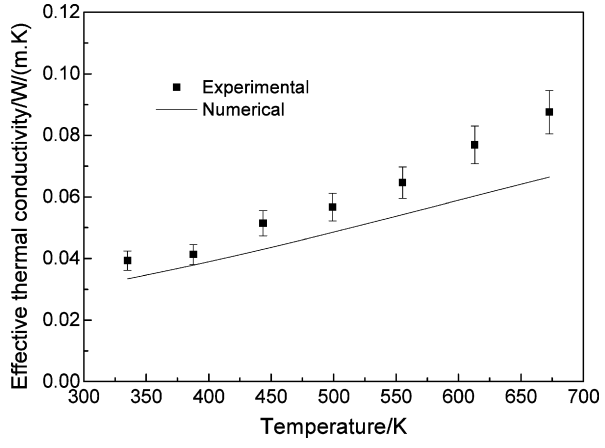

(c)

Fig. 14. Comparison of calculated and measured effective thermal conductivity at nominal pressures (a) 1×10^{-2} Pa; (b) 5×10^3 Pa; (c) 1.013×10^5 Pa.

The comparisons of analytical predictions using the model described above and experimental results of effective thermal conductivity at pressures of 1×10^2 Pa, 5×10^3 Pa and 1.013×10^5 Pa are shown in Figs. 14(a)–14(c). Most of the numerical results under-predicted the experimental results for the sample. An average 14.7 percent difference was obtained between the calculated and measured values for all the testing points. The numerical results agree well with the experimen-

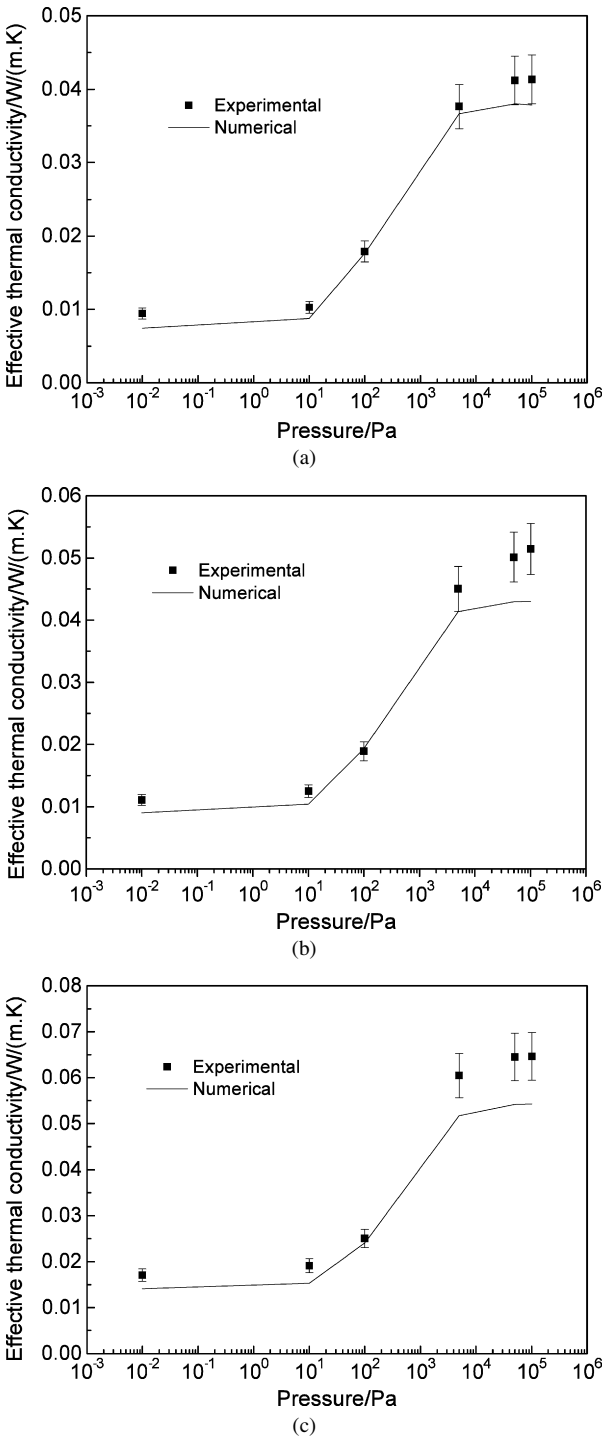

Fig. 15. Comparison of calculated and measured effective thermal conductivity at nominal hot side temperatures (a) 473 K; (b) 573 K; (c) 773 K.

tal results at the nominal pressure of 1×10^2 Pa. The difference at this pressure is less than 4 percent. The comparison of calculated and measured effective thermal conductivity of the sample at nominal hot side temperatures of 473 K, 573 K and 773 K is shown in Figs. 15(a)–15(c). As can be seen from these figures, the largest difference occurs at high temperature, which is almost 26 percent. As for the reasons for the difference, radiation heat transfer is more dominant with the increase of temperature because it is related to the fourth power of temperature. The solution of radiative heat transfer in fibrous insulation is very complicated because of the existence of anisotropic scattering. Therefore, if an improved radiation model taking into account anisotropic scattering by insulation was used to deal with the radiation, the predictions might be more accurate.

5. Conclusions

This work reports on experimental and numerical studies of effective thermal conductivity for high-alumina fibrous insulation. Analytical models combined radiation and conduction heat transfer were developed to predict the effective thermal conductivity of the fibrous insulation at various temperatures and pressures. The optically thick assumption was used to describe the radiation heat transfer through the insulation. The effective thermal conductivities of the fibrous insulation were measured at gas pressures between 10^{-2} Pa and 10^5 Pa and temperatures up to 973 K. The transmittance spectra of the fibrous insulation were also measured at corresponding temperatures. The spectral extinction coefficients and Rosseland mean extinction coefficients were obtained based on transmittance data. The calculated values corresponded to the experimental values within an average of 14.7 percent. The model was consistent with experimental results through the temperatures and pressures under the investigation. Gas conduction is almost negligible below 1 Pa. Solid and radiative contributions in the insulation are found to be independent of pressure. Therefore, gaseous conductivity at high pressures can thus be obtained by subtracting this measured result at low pressures from the total heat transfer. Gas thermal conductivity accounts for about 70 percent of the total effective thermal conductivity when the environmental pressure is larger than 5×10^3 Pa. Suppose that the mean radiative thermal conductivity at the hot side temperature T_1 and the cold side T_2 is defined as

$$\bar{k}_r = \frac{\int_{T_2}^{T_1} (16\sigma/(3K_R(T))T^3)\,dT}{T_1 - T_2},$$

the mean radiative thermal conductivity can reach 1.82×10^{-2} W m^{-1} K^{-1} at the nominal hot side temperature of 973 K, which means that radiative thermal conductivity accounts for about 70–80 percent at low pressures when the gas conduction is almost negligible, while about 20–30 percent at high pressures. Radiation heat transfer and gas conduction are the dominant heat transfer mechanisms under investigated conditions. Therefore, vacuum thermal insulation technology and highly reflective coatings applied on the surface of fibers are good ways to further enhance the heat insulation effect.

Acknowledgements

This work was supported by the National High Technology 863 Projects Foundation of China (No. 2004AA724031).The authors also gratefully acknowledge the financial support of Center for Composite Materials and Structures of HIT in China.

References

[1] K. Daryabeigi, Design of high-temperature multi-layer insulation for reusable launch vehicles, Ph.D. dissertation, University of Virginia, 2000.
[2] S.C. Lee, G.R. Cunnington, Conduction and radiation heat transfer in high porosity fiber thermal insulation, J. Thermophys. Heat Transfer 14 (2) (2000) 121–136.
[3] J.D. Verschoor, P. Greebler, N.J. Manville, Heat transfer by gas conduction and radiation in fibrous insulation, J. Heat Transfer 74 (1952) 467–474.
[4] N.E. Hager, R.C. Steere, Radiant heat transfer in fibrous thermal insulation, J. Appl. Phys. 38 (12) (1967) 4663–4668.
[5] B.K. Larkin, S.W. Churchill, Heat transfer by radiant through porous insulations, AIChE J. 4 (5) (1959) 467–474.
[6] T.W. Tong, C.L. Tien, Radiative heat transfer in fibrous insulations – Part I: Analytical study, J. Heat Transfer 105 (1) (1983) 70–75.
[7] T.W. Tong, S.Q. Yang, C.L. Tien, Radiative heat transfer in fibrous insulations – Part II: Experimental study, J. Heat Transfer 105 (1) (1983) 70–75.
[8] K. Daryabeigi, Analysis and testing of high-temperature fibrous insulation for reusable launch vehicles, AIAA Paper 99-1044.
[9] C. Stark, J. Fricke, Improved heat-transfer models for fibrous insulations, Int. J. Heat Mass Transfer 36 (1993) 617–625.
[10] E.M. Sparrow, R.D. Cess, Radiation Heat Transfer, augmented ed., McGraw-Hill, New York, 1978, pp. 255–271.
[11] R. Siegel, J.R. Howell, Thermal Radiation Heat Transfer, Taylor & Francis, London, 1992.
[12] K. Daryabeigi, Thermal analysis and design of multi-layer insulation for re-entry aerodynamic heating, AIAA Paper 2001-2834.
[13] L. Lees, C.Y. Liu, Kinetic theory description of conductive heat transfer from a fine wire, Phys. Fluids 5 (10) (1962) 1137–1148.
[14] C.Y. Liu, L. Lees, Kinetic Theory Description of Plane Compressible Coquette Flow, Advances in Applied Mechanics, Academic Press, New York, 1961.
[15] E.H. Kennard, Kinetic Theory of Gases, McGraw-Hill Book Company, 1938.
[16] S.D. Williams, D.M. Curry, Predictions of rigid silica based insulation conductivity using morphological data, Presented at the 29th National Heat Transfer Conference, Atlanta, GA, 1993.
[17] K. Daryabeigi, Heat transfer in high-temperature fibrous insulation, AIAA Paper 2002-3332.
[18] Q. Yu, N. Wen, L. Yang, Materials Science Progress 3 (3) (1989) 249–254 (in Chinese).